



Development and Evaluation of Synthetic Paediatric Mid-Thoracic Spine Model for Scoliosis Assessment

by

**Nor Amalina Muhayudin
(1934313045)**

A thesis submitted in fulfillment of the requirements for the degree of
Doctor of Philosophy

**Faculty of Electronic Engineering Technology
UNIVERSITI MALAYSIA PERLIS**

2021

ACKNOWLEDGEMENT

In the name of Allah, the Most Gracious and Most Merciful

Alhamdulillah, all praises belongs to Allah for giving me health, strength and knowledge to complete the research successfully.

I would like to express my deep and sincere gratitude to my research supervisor, Assoc Prof Ir Dr Khairul Salleh Basaruddin for guiding me throughout the process of completing this research. Special thanks to my former supervisors Dr Fiona McEvoy and Mr Anthony Tansey for helping me with this research. I appreciate all the time and effort that each of you invested in assisting me.

I am extremely grateful to my parents for their love, prayers, caring and sacrifices for educating and preparing me for my future. Your prayer and love for me was what sustained me this far. Thank you to my beloved brother, sisters, and aunty for their endless love, prayers and encouragement. I am very much thankful to my besties Liyana and Fatin for the continuing support and just be there throughout my journey to complete this research work.

Thank you everyone. This is a long journey indeed but I finally did it!

©This item is protected by original copyright

TABLE OF CONTENTS

	PAGE
DECLARATION OF THESIS	i
ACKNOWLEDGEMENT	ii
TABLE OF CONTENTS	iii
LIST OF TABLES	vii
LIST OF FIGURES	x
LIST OF ABBREVIATIONS	xix
LIST OF SYMBOLS	xx
ABSTRAK	xxi
ABSTRACT	xxii
CHAPTER 1 : INTRODUCTION	1
1.1 Research Background	1
1.2 Problem Statements and Research Motivation	2
1.3 Research Questions	4
1.4 Research Objectives	5
1.5 Research Scope and Limitations	5
CHAPTER 2 : LITERATURE REVIEW	7
2.1 Introduction	7
2.2 Scoliosis	7
2.2.1 Diagnosis of Scoliosis	8
2.2.2 Measurement of Scoliosis	9

2.3	Spinal Anatomy	11
2.3.1	Vertebrae	12
2.3.2	Intervertebral Disc	15
2.3.3	Spinal Ligaments	16
2.4	Spinal Biomechanics	18
2.4.1	Vertebral Trabecular Bone	18
2.4.2	Vertebral Cortical Bone	20
2.4.3	Intervertebral Disc	21
2.4.4	Spinal Ligaments	22
2.5	Biomechanics of Paediatric Spine	27
2.6	Biomechanics of Animal Cadaveric Spine	30
2.7	Synthetic Spine Development	36
2.7.1	Materials of Synthetic Spine	36
2.7.2	Physical Model of Synthetic Spine	39
2.7.3	3D Printed Synthetic Spine	40
2.8	Statistical Analysis	44
2.9	Finite Element Modelling (FEM) of Spine	44
2.9.1	FE Models of the Vertebra	45
2.9.2	FE Models of Intervertebral Disc	48
2.9.3	Models of Spine Segment	49
2.9.4	FE Models of Paediatric Spine	51
2.10	Summary	56
CHAPTER 3 : RESEARCH METHODOLOGY		59
3.1	Introduction	59
3.2	Research Flow	59
3.3	Materials Selection of Synthetic Paediatric Spine Components	62
3.3.1	Mechanical Properties of Vertebral Trabecular Bone	62

3.3.2	Microstructure Characterisation of Synthetic PU Foams	64
3.3.3	Mechanical Properties of Vertebral Cortical Bone	67
3.3.4	Mechanical Properties of Vertebral Body	69
3.3.5	Mechanical Properties of Intervertebral Disc	70
3.3.6	Mechanical Properties of Spinal Ligaments	73
3.4	Fabrication of Synthetic Paediatric Spine	78
3.5	Biomechanical Testing of Porcine Spine and Synthetic Paediatric Spine	83
3.5.1	Specimen Preparation of Porcine Spine	83
3.5.2	Experimental Set Up of Porcine Spine	85
3.5.3	Specimen Preparation of Synthetic Paediatric Spine	86
3.5.4	Experimental Set Up of Synthetic Paediatric Spine	87
3.6	Finite Element Analysis of Paediatric Spine	88
3.6.1	Development of the Paediatric Spine Model	88
3.6.1.1	Posterior Element	91
3.6.1.2	Vertebral Column	93
3.6.2	Mesh Development	93
3.6.2.1	Spinal Column	94
3.6.2.2	Posterior Element	95
3.6.2.3	Spinal ligaments and facet joints	96
3.6.3	Loading and Boundary Conditions	98
3.6.4	Material Properties	99
3.6.5	Validation of Finite Element Model	102
3.7	Summary	105
CHAPTER 4 : MODEL DEVELOPMENT AND BIOMECHANICAL TESTING OF SYNTHETIC PAEDIA TRIC SPINE		106
4.1	Introduction	106

4.2	Selected Materials of Synthetic Paediatric Spine Components	106
4.2.1	Mechanical Properties of Vertebral Trabecular Bone	106
4.2.2	Mechanical Properties of Vertebral Body	121
4.2.3	Mechanical Properties of Intervertebral Disc	122
4.2.4	Mechanical Properties of Spinal Ligaments	127
4.3	Fabricated Synthetic Paediatric Spine	130
4.4	Range of Motion under Biomechanical Testing	131
4.4.1	ROM of Porcine Spine	131
4.4.2	ROM of Synthetic Paediatric Spine	139
4.4.3	Comparison of ROM between Porcine and Synthetic Paediatric Spine	146
4.5	Summary	148
CHAPTER 5 : FINITE ELEMENT ANALYSIS OF SYNTHETIC PAEDIATRIC SPINE		149
5.1	Introduction	149
5.2	ROM of Paediatric Synthetic Spine under Finite Element Analysis	149
5.3	Comparison of ROM between FEA and Experiment of Synthetic Paediatric Spine	154
5.4	Stress Distribution of Intervertebral Disc under Loading Conditions.	163
5.5	Summary	171
CHAPTER 6 : CONCLUSION, MODEL LIMITATIONS AND FUTURE RECOMMENDATIONS		173
6.1	Conclusion	173
6.2	Model Limitations	179
6.3	Recommendations for Future Works	180
REFERENCES		182
LIST OF PUBLICATIONS		194

LIST OF TABLES

	PAGE
Table 2.1 Comparison of the vertebral body, spinal canal and pedicle between animals and human (Sheng et al., 2010).	31
Table 2.2 Age and the average weight of animal used (Bozkus et al., 2005; Kumar et al., 2002; Wilke et al., 1997).	31
Table 2.3 Summary of gap analysis in this research.	58
Table 3.1 Summary of apparent density; average cell size and mean intercept length of three different densities (0.16 g/cm ³ , 0.24 g/cm ³ and 0.42 g/cm ³).	65
Table 3.2 Comparison data between current testing and technical data from the supplier of monothane® with human data.	71
Table 3.3 Compression Moduli and hardness values for the type of silicone used as nucleus pulposus.	72
Table 3.4 Size comparison between all spine models in this study	79
Table 3.5 Specimen number, mass and age of the porcine spines used in the experiment.	84
Table 3.6 Meshing specifications for each component in the FE model.	98
Table 3.7 Material Properties of paediatric material linear and nonlinear.	100
Table 3.8 Material properties of synthetic material.	102
Table 3.9 Material Properties of adult and paediatric model.	104

Table 4.1	Mechanical properties for 0.16 g/cm ³ and 0.24 g/cm ³ for 25 mm diameter and 50 mm height of expandable PU foam specimens.	108
Table 4.2	Mechanical properties for 0.16 g/cm ³ , 0.24 g/cm ³ and 0.42 g/cm ³ for 9 mm diameter and 7.7 + 0.2 mm height of expandable PU foam specimens.	108
Table 4.3	Mechanical properties of porcine trabecular core specimens.	109
Table 4.4	Mechanical properties for the current study versus Thompson et al. (2003) and Domann et al. (2011) for various densities of PU foams.	111
Table 4.5	Current study (larger specimen) versus human trabecular bone as presented in literature.	113
Table 4.6	Current study versus Patel et al. (2008) for 0.16, 0.24, 0.32 and 0.42 g/cm ³ PU foams (smaller specimen).	116
Table 4.7	Current study of porcine spine versus Teo et al. (2006).	119
Table 4.8	Comparison of axial stiffness between current study and literature.	122
Table 4.9	Compression moduli, stiffness and strain values for paediatric AID with different silicones as nucleus pulposus.	123
Table 4.10	Average results from 8 design points.	124
Table 4.11	Comparison of compression modulus and stiffness of current study with AID and the human thoracic disc from literature.	126
Table 4.12	Comparison of NZ and EZ stiffness between literature and current study.	129
Table 4.13	Materials selected for each component in spine to fabricate synthetic paediatric spine.	131

Table 4.14	The data of the ROM for each DOF of each specimen.	134
Table 4.15	Data of the ROM and S1/S2 for each motions of synthetic paediatric specimen at $\pm 4\text{Nm}$.	139
Table 4.16	Comparison of hysteresis curve between synthetic paediatric spine and analogue adult lumbar spine from Sawbones®	145
Table 5.1	Summary of ROM results for all models under various moments.	161
Table 5.2	Comparison between human adult, synthetic paediatric spine and paediatric FE model in flexion extension.	168
Table 5.3	Comparison between human adult, synthetic paediatric spine and synthetic paediatric FE model in lateral bending and axial rotation.	169

©This item is protected by original copyright

LIST OF FIGURES

	PAGE	
Figure 1.1	Illustration of spinal shape for (a) normal spine and (b) spine with scoliosis. (Erika, 2017)	1
Figure 2.1	Three main planes in spinal anatomy (Bridwell, 2017).	8
Figure 2.2	Scoliosis screening methods. (A) Adam's test from posterior view (Farhaan et al., 2013) and (B) Scoliometer (Hresko, 2013).	9
Figure 2.3	Measurement of Cobb angle on X-Ray from Hresko (2013) and Yizhar & Dalia (2009).	10
Figure 2.4	Anatomy of the spine from lateral and posterior view (Bridwell, 2019).	12
Figure 2.5	The difference between adult and paediatric thoracic vertebrae (a) adult spine (b) paediatric spine (Weinstein, 2001).	13
Figure 2.6	(a) Vertebral morphometry measurements were performed on midsagittal T1-weighted MR images of the thoracic spine. (b) Illustration of vertebral landmarks from which vertebral shape parameters were defined. Marked points represent the 4 vertebral corners and midpoints of the endplates, while 'D' represents the anteroposterior vertebral diameter (Goh et al., 2000).	14
Figure 2.7	(a) Digitizing landmarks on anterior-posterior and lateral vertebrae. (b) Lateral vertebral dimensions from the digitised points (Schober et al., 2012).	15

Figure 2.8	Structure of the intervertebral disc (White & Panjabi, 1990).	16
Figure 2.9	Spinal ligaments surrounded functional spinal unit.	17
Figure 2.10	Structure of bone from (a) young and (b) elderly specimens (Domann, 2011; Mosekilde et al. 1987).	19
Figure 2.11	The comparison structure between the paediatric and mature spine (Boos et al., 2002).	22
Figure 2.12	Typical load-displacement or stress-strain curve for a ligament in tension (White & Panjabi, 1990).	23
Figure 2.13	Load deformation behaviour of spinal ligaments in tension (White & Panjabi, 1990).	24
Figure 2.14	The schematic by Yoganandan et al. was obtained by tracing the actual cryomicrotome section, and lines were drawn to describe the lengths (Yoganandan et al., 2001).	25
Figure 2.15	Test apparatus used by Ouyang for flexion extension and lateral bending (Ouyang et al., 2005).	28
Figure 2.16	Anatomical parameters measured. (I) Vertebral body height anterior (VBHv), (J) vertebral body height posterior (VBHd) (Dath et al., 2007).	30
Figure 2.17	Typical sigmoidal curve of spine range of motion (ROM). The arrows indicated the loading and unloading direction. The information highlighted are the total ROM, neutral zone (NZ) ROM, neutral zone (NZ) stiffness and extension zone (EZ) stiffness (Wilke et al., 2011).	32
Figure 2.18	Comparison in ROM between pig, calf, sheep and human spine at (a) flexion and extension (b) lateral bending right and left (c) axial rotation right and left (Wilke et al., 2011; Wilke et al., 1997).	34

Figure 2.19	Comparison between human and porcine spine in the segment. (Busscher et al., 2010).	35
Figure 2.20	Stress distribution in the porcine lumbar disc by Ryan et al.(2008).	36
Figure 2.21	A typical stress-strain curve for the trabecular curve at various relative densities (White & Panjabi, 1990).	39
Figure 2.22	Anterior view photo, anterior view x-ray and lateral view x-ray imaging of different sample conditions (Wang et al., 2014).	40
Figure 2.23	Screenshot of a 3D-rendering of the L3-L5 segment model. Blue indicates model components to be printed to mimic bone, and orange indicates components to be printed to mimic ligamentous structures (Bohl et al., 2018).	41
Figure 2.24	Four different synthetic spine models shown (left to right) in anterior, right lateral, posterior, and left lateral views (Bohl et al., 2019).	42
Figure 2.25	Synthetic spine models D and E compared with mean data for cadaveric controls with respect to (A) flexion-extension, (B) lateral bending, and (C) axial rotation range of motion (ROM) at 7.5Nm and (D) axial compression. Error bars indicate standard deviation. (Bohl et al., 2019).	43
Figure 2.26	(a) Overall model geometry. Vertebral body height (BH), width (W), and depth (D), as well as shell thickness (TL) and wall curvature (S). (Whyne et al., 2003).	47
Figure 2.27	Finite element mesh of 1/4 of an intervertebral disc with differentiation in the nucleus pulposus (orange) and the annulus fibrosus (red), in the stress-free state by Schroeder et al.(2006).	48

Figure 2.28	Simplified geometry parameters of the L3–L4 segment (Niemeyer et al., 2012).	50
Figure 2.29	Multi segments model of thoracolumbar region (T11- L5) (Tyndyka et al., 2007).	51
Figure 2.30	Different views of finite element mesh of ligamentous adult C4–C5–C6 spine from Kumaresan et al. (2000).	53
Figure 2.31	L1–S1 finite element model representing an eight-year-old paediatric human spine from scaling up adult model by 141% (Jebaseelan et al., 2010).	54
Figure 3.1	Flow chart of the overall process taken in this study.	61
Figure 3.2	Bone core specimens drilled from the porcine vertebra (Morgan & Keaveny, 2001).	64
Figure 3.3	SEM images of expandable rigid PU foam of three different densities at 500 μm scale bar (a) 0.16 g/cm^3 (b) 0.24 g/cm^3 and (c) 0.42 g/cm^3	66
Figure 3.4	Mechanical testing setup of foams and porcine trabecular core sample.	67
Figure 3.5	The sequence steps to fabricate cortical bone.	69
Figure 3.6	Compression test set up for the synthetic vertebral body.	70
Figure 3.7	Design and exploded view of the complete artificial intervertebral disc (AID).	71
Figure 3.8	The 45-degree bias direction of the fibre tape.	73
Figure 3.9	The fibre tape was clamped at both ends of the mould.	74
Figure 3.10	The schematic diagram of the synthetic ligament.	75

Figure 3.11	Typical load-displacement curve of the synthetic spinal ligament.	78
Figure 3.12	Process flow of scale-up synthetic paediatric spine.	80
Figure 3.13	The process flow to manufacture paediatric synthetic spine from (a) cortical (b) completed vertebra (c) disc (d) assemble ALL and PLL (e) added posterior ligaments and (f) completed FSU	81
Figure 3.14	The hierarchical chart of the fabricated synthetic paediatric spine.	82
Figure 3.15	The specimens used with the ribs and spinous process removed.	84
Figure 3.16	The specimens were dissected into single FSU's.	84
Figure 3.17	The upper half of the top vertebra and the lower half of the bottom vertebra were embedded in the liquid plastic.	85
Figure 3.18	The specimens fixed in the spine simulator.	86
Figure 3.19	Synthetic paediatric spine was potted in the liquid resin.	87
Figure 3.20	Synthetic paediatric spine was fixed in the MTS Bionix Servo Hydraulic spine simulator.	88
Figure 3.21	The overall flow to develop the paediatric spine finite element model.	90
Figure 3.22	The schematic diagram represents the steps taken to create the complete vertebra.	92
Figure 3.23	Diagram to show the process to generate vertebral column; (a) the reference spinal curvatures from human spine CAD model, (b) the vertebral column from T4-T8 with added disc, (c) the vertebral column from posterior view.	93

Figure 3.24	Criss cross pattern embedded within the annulus matrix.	94
Figure 3.25	4 noded tetrahedral elements in posterior element.	95
Figure 3.26	Tetrahedral elements were connected with brick elements of vertebral body at pedicle.	95
Figure 3.27	Stress distribution transition from vertebral body to posterior elements.	96
Figure 3.28	Completed multi segment model of T4-T8.	97
Figure 3.29	An example of FSU model (T4-T5), which was used to perform further analysis.	97
Figure 3.30	Loading and boundary conditions of all FE models.	99
Figure 3.31	Displacements of linear versus nonlinear material under ± 0.5 Nm.	101
Figure 4.1	Typical stress-strain graphs for expandable polyurethane foams tested using 25 mm diameter and 50 mm height specimens for 0.16 and 0.24 g/cm ³ densities.	107
Figure 4.2	Typical stress-strain graphs for expandable polyurethane foams tested using 9 mm diameter and 7.7 ± 0.2 mm specimens for 0.16, 0.24 and 0.42 g/cm ³ densities.	107
Figure 4.3	Linear interpolation of average values extracted from Patel et al. (2008) for 0.24 and 0.42 g/cm ³ for compression modulus and yield stress.	115
Figure 4.4	Compression modulus of synthetic PU foam, human trabecular bone and porcine trabecular bone between current study and various literature, (Banse, Sims, 2002; Domann, 2011; Kopperdahl & Keaveny, 1998; Morgan & Keaveny, 2001; Teo et al., 2006).	120

Figure 4.5	Load-displacement of porcine spine (T4-T5) and synthetic spine (T4-T5)	122
Figure 4.6	Stress versus strain for the paediatric artificial intervertebral disc with different silicones as nucleus pulposus.	123
Figure 4.7	Main effects and interactions for all factors.	125
Figure 4.8	Stress strain curve of fibre tape.	128
Figure 4.9	Sample of fabricated FSU synthetic paediatric spine of T4-T5.	130
Figure 4.10	Typical flexion extension of porcine spine.	132
Figure 4.11	Typical lateral bending of porcine spine.	133
Figure 4.12	Typical axial rotation of porcine spine.	133
Figure 4.13	Flexion extension of porcine ROM between the current study and Wilke et al. (2011) at ± 7.5 Nm moments.	135
Figure 4.14	Lateral bending of porcine ROM between the current study and Wilke et al. (2011) at ± 7.5 Nm moments.	136
Figure 4.15	Axial rotation of porcine ROM between the current study and Wilke et al. (2011) at ± 7.5 Nm moments.	136
Figure 4.16	Overall porcine ROM of mid thoracic region (T4-T8) between current study versus Wilke et al. (2011) at ± 7.5 Nm moments.	137
Figure 4.17	Comparison between porcine spine from current study and Wilke et al. (2011) with human adult spine from White and Panjabi (1990).	138
Figure 4.18	Flexion extension of synthetic paediatric spine for all FSUs.	140
Figure 4.19	Lateral Bending of synthetic paediatric spine for all FSUs.	140

Figure 4.20	Axial rotation of synthetic paediatric spine for all FSUs.	141
Figure 4.21	Overall ROM of synthetic paediatric spine at ± 4 m.	143
Figure 4.22	Synthetic paediatric spine versus porcine spine at ± 4 Nm moments.	147
Figure 5.1	An example of ROM contour on the FE model.	150
Figure 5.2	Comparison of ROM between FE model results with an invitro study of human adult conducted by White and Panjabi (1990) at ± 7.5 Nm.	151
Figure 5.3	The geometrical effect with difference geometrical size between adult geometry with paediatric geometry using adult material properties under ± 7.5 Nm.	153
Figure 5.4	The material effect with difference material properties between adult geometry (AG) with paediatric geometry (PG) under ± 7.5 Nm.	153
Figure 5.5	ROM of thoracic paediatric spine FE model at ± 0.5 Nm.	155
Figure 5.6	ROM of in-vitro study of thoracic adult spine by White and Panjabi (1990) at ± 7.5 Nm.	155
Figure 5.7	The synthetic model (SM) (200%) results from $\pm (1$ to $4)$ Nm versus paediatric model (PM) (100%) at ± 0.5 Nm.	157
Figure 5.8	FE model versus experimental data of synthetic paediatric model (200%) at ± 2 Nm.	158
Figure 5.9	FE model versus experimental data of synthetic paediatric model (200%) at ± 3 Nm.	158
Figure 5.10	FE model of paediatric model at ± 0.5 Nm versus experimental data of synthetic paediatric spine (200%) at ± 2 Nm.	160

Figure 5.11	FE model of paediatric model at ± 0.5 Nm versus experimental data of synthetic paediatric spine (200%) at ± 3 Nm.	160
Figure 5.12	The experimental data of synthetic paediatric that matched the ROM of paediatric FE model at ± 0.5 Nm.	163
Figure 5.13	Lateral bending right that was conducted on both models.	164
Figure 5.14	Stress distribution of human adult FE model between human disc and synthetic disc in two positions.	165
Figure 5.15	The ROM of synthetic paediatric spine from ± 2 Nm to ± 4 Nm.	171

©This item is protected by original copyright

LIST OF ABBREVIATIONS

ROM	Range of Motion
FE	Finite Element
FEA	Finite Element Analysis
FEM	Finite Element Modelling
LF	Ligamentum Flavum
ISL	Interspinous Ligament
TL	Intertransverse Ligament
ALL	Anterior Longitudinal Ligament
PLL	Posterior Longitudinal Ligament
SSL	Supraspinous Ligament
CL	Capsulary Ligament
PVC	Polyvinyl Chloride
PU	Polyurethane
ASTM	American Standard for Testing & Materials
NZ	Neutral Zone
PZ	Plastic Zone
FSU	Functional Spinal unit
EZ	Elastic Zone
CT	Computed Tomography
DOF	Degree of Freedom
SEM	Scanning Electron Microscope
AID	Artificial Intervertebral Disc
SLS	Selective Laser Sintering
AD	Age Density

LIST OF SYMBOLS

C	Cervical spine region
T	Thoracic spine region
L	Lumbar spine region
S1	Slope 1
S2	Slope 2
L_L	Length of cell
N_L	Number of cell
ρ_c	Density of the composite
ρ_m	Density of the matrix
ρ_f	Density of the fibre
ρ_{C1}	Density of the fabricated composite

©This item is protected by original copyright

Pembangunan dan Penilaian Model Tulang Belakang Pertengahan Toraks Pediatrik Sintetik untuk Pentaksiran Skoliosis

ABSTRAK

Skoliosis adalah kelengkungan melintang tulang belakang yang tidak normal, walaupun semua peringkat usia boleh mengalami skoliosis, penyakit ini biasanya dihidapi oleh kanak-kanak. Sebilangan besar kajian yang mengkaji kes skoliosis menggunakan tulang belakang haiwan dan dewasa, yang sebenarnya tidak mewakili tulang belakang pediatrik kerana pediatrik bukan miniatur tulang belakang dewasa. Oleh itu, tujuan kajian ini adalah untuk membangunkan model tulang belakang pediatrik sintetik dan menilai tingkah laku mekanikal berbanding dengan tulang belakang dewasa dan haiwan. Bahagian tulang belakang yang dipilih untuk penyelidikan ini adalah kawasan pertengahan toraks dari T4-T8. Oleh kerana tulang belakang adalah struktur yang kompleks, proses fabrikasi model sintetik dipermudah dengan memfokuskan pada tiga komponen utama, iaitu vertebra, cakera intervertebral dan ligamen. Span PU yang boleh dikembangkan dipilih untuk menggantikan tulang trabekular. Manakala untuk cakera intervertebral bahan dipilih adalah silikon bagi menggantikan nukleus pulposus dan monothane® sebagai annulus fibrosus. Bahan komposit yang terdiri daripada pita serat dan silikon plastik digunakan untuk mewakili ligamen. Tulang belakang pediatrik sintetik dibuat dengan membesarkan saiz model tulang belakang pediatrik sebanyak 200%. Ujian biomekanik dilakukan untuk mengukur julat pergerakan dan ketidaklurusan lengkung sigmoidal pada enam darjah kebebasan dengan momen antara ± 1 hingga ± 4 Nm. Hasilnya dibandingkan dengan tulang belakang khinzir dan tulang belakang dewasa analog (Sawbones®). Perbezaan yang terdapat pada pergerakan melintang dan putaran paksi tulang belakang pediatrik sintetik berbanding khinzir adalah 18% dan 3% sementara pergerakan fleksi tegangan berbeza sebanyak 45% tetapi masih berada dalam julat. Lengkung sigmoidal serupa diperhatikan untuk keenam-enam darjah kebebasan jika dibandingkan dengan tulang belakang lumbar dewasa analog, di mana fleksi tegangan dan putaran paksi cenderung lebih lurus. Julat pergerakan pediatrik diukur menggunakan model unsur terhingga (FE) pediatrik yang disahkan pada momen ± 0.5 Nm (beban pediatrik) untuk menentukan momen yang diperlukan oleh tulang belakang pediatrik sintetik bagi mendapatkan julat pergerakan pediatrik. Hasil kajian menunjukkan bahawa dalam fleksi tegangan, julat pergerakan pediatrik mendekati momen ± 3 Nm, sementara pada pergerakan melintang dan putaran paksi, ROM pediatrik lebih dekat dengan momen ± 2 Nm. Pergerakan tulang belakang pediatrik sintetik didapati lebih lentur dalam fleksi tegangan dan lebih fleksibel dalam lenturan melintang berbanding dengan model FE pediatrik. Ini berkemungkinan disebabkan reka bentuk cakera intervertebral yang dipermudah dan ikatan yang lemah antara cakera dan tulang belakang. Walaupun begitu, model yang difabrikasi menunjukkan hasil yang positif dan menunjukkan bahawa tulang belakang pediatrik sintetik berpotensi untuk digunakan sebagai alternatif model tulang belakang pediatrik dan dalam jangka panjang dapat menggantikan tulang belakang haiwan dan dewasa untuk kajian patologi tulang belakang pediatrik seperti skoliosis.

Development and Evaluation of Synthetic Paediatric Mid-Thoracic Spine Model For Scoliosis Assessment

ABSTRACT

Scoliosis is a condition with abnormal spine lateral curvature that is affecting people of all ages but is the most common in children. Most of the studies that had investigated scoliosis-related subjects were using animal and adult spines; thus, in reality, they may not be representing the paediatric spine, as the paediatric spine is not the same and should not be treated as a miniature version of an adult spine. Therefore, the aim of this study is to develop a synthetic paediatric spine model and to evaluate the mechanical behaviour of the paediatric spine in comparison with adult and animal spines. The section of the spine selected for this research was the T4 to T8 mid-thoracic region. As the spine is such a complex structure, the fabrication process of the synthetic model was simplified by focusing on three main components; vertebra, intervertebral disc and spinal ligaments. The expandable PU foam was selected to replicate the trabecular bone. Meanwhile, the lightweight silicone materials were selected to model the intervertebral disc by replicating the nucleus pulposus, while the monothane® materials were used to model the annulus fibrosus. Additionally, the composite materials consisting of fibre tape and plastic silicone were used to represent the spinal ligaments. The synthetic paediatric spine was fabricated as a scaled-up model of the paediatric spine by 200%. Biomechanical tests were conducted to measure the range of motion (ROM) and non-linearity of the sigmoidal curves at six DOF, with moments ranging from between ± 1 to ± 4 Nm. The results were compared with the data reported on porcine spines (retrieved from prior literature) and an analogue adult lumbar spine (Sawbones®). The differences of 18% and 3%, respectively, were found in lateral bending and axial rotation of the synthetic paediatric spine, as compared to the porcine spine. Moreover, the flexion extension was observed to differ by 45%, but the ROM was still within the range. Similar sigmoidal curves were observed for all six DOF when compared to the analogue adult lumbar spine, where the flexion extension and axial rotation tended to be more linear. The paediatric ROM was measured using a validated paediatric FE model at ± 0.5 Nm moment (i.e. paediatric loading) to determine the moment required by the synthetic paediatric spine to obtain the paediatric ROM. The results showed that in flexion extension, the paediatric ROM was closer to ± 3 Nm moment, while in the lateral bending and axial rotation, the paediatric ROM was closer to ± 2 Nm moment. The movements of the synthetic paediatric spine were found to be stiffer in the flexion extension but were more flexible in the lateral bending in comparison to the paediatric FE model. This was potentially due to the simplified design of the intervertebral disc, as well as the poor bonding between the disc and vertebrae. Despite that, the developed model showed promising results, hence suggested that the synthetic paediatric spine has the potential application as an alternative paediatric spine model. In the long term, this model could replace the animal and adult spines to investigate pathologies of the paediatric spine, such as scoliosis.

CHAPTER 1 : INTRODUCTION

1.1 Research Background

This present study is evolved from original research that measures spinal curvature, better known as scoliosis. Scoliosis can be characterised by a side-to-side deviation from the normal body axis and is caused by the lateral displacement of the spine (Ali Baaj, 2017), as illustrated in Figure 1.1. People of all ages can develop scoliosis, but this issue is more prevalent in children. Depending on the severity of curvature and the age of a person, scoliosis treatment is typically divided into three major phases, which are observation, bracing, and surgery for very severe cases.

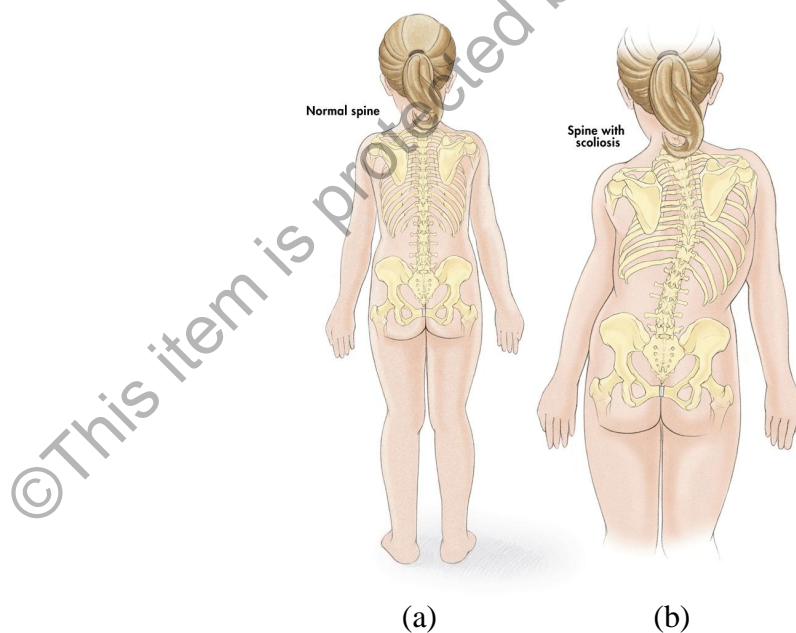


Figure 1.1 Illustration of spinal shape for (a) normal spine and (b) spine with scoliosis. (Erika, 2017)

In Malaysia, 55.8 % of students from a sample size of 9000 from the ages of between 13 to 15 years old were positively diagnosed to have suffered from scoliosis, based on a school screening programme conducted by Deepak et al. (2017), while around 2.6% of these students were severely affected, with the Cobb angle of more than 40 degree recorded. In Asian countries, adolescent idiopathic scoliosis had a prevalence of about 0.4% to 7% (Deepak et al., 2017; Du et al., 2016; Suh et al., 2011). These data revealed the common prevalence of scoliosis among children. Most importantly, surgical treatments that are costly and risky for a child's development are required to treat severe scoliosis cases.

The cost of spinal surgery treatments is very high and often prohibitive. The study by Yawn & Yawn (2000) calculated the estimated scoliosis surgical costs in the United States and revealed that an average cost of \$120,000 was needed per operation, based on the data collected from approximately 20,000 Harrington rod implantation surgeries that were performed on the patients with scoliosis annually. Another issue is that approximately 8,000 peoples have been legally defined as permanently disabled for the rest of their lives after they had undergone scoliosis corrective surgeries in their youth.

1.2 Problem Statements and Research Motivation

Scoliosis surgical treatment is expensive and has a high failure risk during the surgery due to the usage of screws and rods. Although numerous studies (Janssen et al., 2011; Lavell et al., 2016; Nowak, 2019; Patel et al., 2011; Schwab et al., 2009) have been performed to investigate these associated problems of scoliosis surgical